Int. J. Advanced Design and Manufacturing Technology, 2025, Vol. 18, No. 3, pp. 25-42

DOI: ***ISSN: 2252-0406*** ***https://admt.isfahan.iau.ir***

Advanced Modeling and Analysis of Diesel Engine Test Support Structure (ETSS) Using (FEM) and (XFEM): A Comprehensive Study on Fracture Mechanics, Fatigue Life, and Modal Analysis of Crack Growth

Mohammad Mohammadi
M.Sc. student in Mechanical Engineering and Top Researcher at the Young Researchers and Elite Club, Sh. C., Islamic Azad University, Shiraz, Iran

Seyed Mohammad Reza Nazemosadat *, Ahmad Afsari
Department of Mechanical Engineering, Sh. C., Islamic Azad University, Shiraz, Iran
E-mail: smr.nazemosadat@iau.ac.ir, reza_nazemsadat@yahoo.com
*Corresponding author

Received: 19 April 2025, Revised: 26 May 2025, Accepted: 20 October 2025

Abstract: The Engine Test Support Structure is vital in testing engines and enhancing technician safety across various industries. This study proposed and modeled a steel structure using INVENTOR software. Subsequently, static analysis, modal vibration analysis, safety factor analysis, fracture mechanics, fatigue life analysis, and modal crack growth analysis were performed on this structure using ABAQUS software. The static analysis results showed that the von Mises stress in the telescopic support of the engine handle and the longitudinal and transverse chassis ranged between approximately 275 MPa and 617 MPa. In contrast, the minimum von Mises stress was approximately 100 MPa in the plate holding the radiator, fuel tank, and control panel. The modal vibration analysis indicated that the maximum displacement in the longitudinal and transverse chassis areas, engine block, and radiator holder was 0.08135 mm at 7.20 Hz. In contrast, the minimum displacement in the control panel, fuel tank, and battery holder was 0.05419 mm at 9.45 Hz. The fracture mechanics and XFEM analysis showed that areas with a value of 1.0 indicated fully developed cracks and the highest level of discontinuities, suggesting good resistance to fracture. Additionally, the modal crack growth analysis results showed that the maximum crack growth was 0.014 mm under a force of 12 KN, while the minimum crack growth was 0.08 mm under a force of 2 KN. The fatigue life analysis indicated that under a force ranging from 0 to 10 KN over 15 cycles, the structure exhibited good toughness and strength against cyclic loading at critical points. The safety factor analysis revealed that the central longitudinal and transverse floor frames (Body 5) require reinforcement and optimization due to having a safety factor of less than 1.0. A safety factor range of 1.5 to 3 is recommended for these areas, while other components do not require reinforcement.

Keywords: Buckling, Diesel Engine Test Support Structure, Extended Finite Element Method, Fatigue Life Evaluation, Finite Element Method, Fracture Mechanics, Modal Analysis

Biographical notes: Mohammad Mohammadi is a master's student in Mechanical Engineering with a specialization in Applied Design at Islamic Azad University, Shiraz Branch. **Seyed Mohammad Reza Nazemosadat** received his PhD in Mechanical Engineering of Biosystem from Shahrekord University in 2022. **Ahmad Afsari** received his PhD from Delhi Institute of Technology University, India in 1998.

Research paper

1 INTRODUCTION

The Engine Test Support Structure (ETSS) is crucial and applicable to various industries, including automobile manufacturing, shipping, road construction, rail and air transportation, and the military sector. This structure is fundamental due to its use in testing and repairing engines and increasing work safety for technicians. One of the prominent advantages of the supporting structure is cost savings and ease of controlling multiple critical parameters of the diesel engine before its installation and commissioning. This makes it possible to be informed about the occurrence of numerous problems in the engine and to prevent a sudden accident. The support structure is a suitable solution for testing and starting the engine before it is installed in the vehicle, and it enables the technician to identify and solve possible problems, make final adjustments, and repair failures due to removal, rebuilding, re-installation, and modifications before engine installation. Also, considering that the engine is likely to be opened and closed several times to fix its faults, the support structure is expected to save time and service costs by reducing the repetition of the opening and closing process. This structure features bases that accommodate both internal and external installation, as well as support four-, six-, and even eight-cylinder engines. Using the structure, fixing and installing the engine independently in front, back, and even vertical directions is possible.

Koch and Zeller [1] conducted a study titled "Test Stand for Dynamic Investigations of Combustion Engines." The study aimed to optimize the control of combustion engines to achieve the best power and fuel economy within the legislated emission constraints. The study highlighted that achieving this goal required comprehensive experimental investigations. These expenses increased further when considering non-stationary operating conditions and the control of transient behavior, which posed a significant challenge, especially with the methods of optimum control theory and the potential provided by digital electronics and micro-computers.

As an experimental tool for non-stationary engine calibration, BMW installed a "dynamic engine test stand" capable of simulating all non-stationary operating conditions in the field. The test stands mainly comprised a torque-controlled electrical asynchronous motor that generated the torque load at the crankshaft of the combustion engine, a multi-micro-computer system for modeling the vehicle and driver to simulate the driveline load, and a system controller that enforced time histories of torque and revolutions per minute of the test engine to match the simulated values of the vehicle within the required dynamic range. After comprehensive tests were conducted to evaluate the dynamic qualities of the test bed itself, the dynamic testing of the engine in comparison to field tests was investigated.

Von Thun [2] published a study titled "A New Dynamic Combustion Engine Test Stand with Real-Time Simulation of the Vehicle Drive Line." This study introduced a new tool for developing engines and engine control systems. This dynamic test stand aimed to substantially reduce the need to install engines in prototype vehicles and conduct road tests. This control system enabled correct engine loading during transient operations, similar to those in actual cars. The system featured high dynamic response and excellent system stability. The paper compared the drive line simulation with conventional engine test stands. The principles of real-time simulation of the vehicle's spring-mass system were explained using mathematical models and functional block diagrams. Additionally, the criteria used in selecting the design of this system were presented, and the results from test stands in commercial operation were demonstrated.

Voigt [3] published a paper titled "A Control Scheme for a Dynamical Combustion Engine Test Stand" at the International Conference on Control (Control'91). This paper describes the essential components of a control scheme for a dynamic combustion engine test stand. A model of the dynamometer, obtained through theoretical modeling and parameter estimation techniques, was used to design a torque regulator and simulate different control schemes. The time delay of the current converter had a determining influence on the achievable simulation quality. A minor time delay allowed for improved torque control behavior and fewer stability issues within the closed simulation loop. Therefore, control performance could be enhanced by replacing the digitally controlled current converter with an analogue-controlled one.

Modern combustion engines are characterized by an increasing number of cylinders and decreasing moment of inertia. Higher and higher simulated resonance frequencies were demanded. Improving the performance of dynamometer torque control was the only way to attain that goal. The entire control scheme was implemented on a VMEbus computer system, consisting of a central processor with a Motorola 68020, analog and digital I/O boards, and a slave processor with graphical I/O facilities for user interface purposes.

Temple et al. [4] presented a paper titled "Testability Modeling and Analysis of a Rocket Engine Test Stand" at the IEEE Aerospace Conference. This paper describes a testability analysis methodology that enhances the efficiency of maintainability and availability in a system, improves the system's overall capabilities, and provides historically verifiable data to compare testability analysis metrics with observed

discrepancy reports. The paper discusses the methodology of using a testability analysis tool to aid in designing and developing a health management system. It also briefly explains how the model's testability output metrics can be used alongside other model outputs for optimization. Some top-level figures of merit are examined to verify that the testability analysis data are adequate and valid. This technology demonstrated its ability to improve maintenance efficiency and aid in automating an Integrated Vehicle Health Management (IVHM) system while reducing the need for human interaction in decision-making, data acquisition, and testing. The technology also identified critical components in the system and provided a fast and accurate method for fault detection and isolation, diagnosing faults to the lowest level of ambiguity.

The safety, reliability, and testability metrics identified in this study helped reduce the test stand operator's stress levels by increasing confidence in the operational state of the system, especially concerning critical components, both before and during tests. Consequently, confidence in the test stand's output data from the test article was achieved. The study also proved that this technology enhances the sustainability of the test stand, going beyond merely meeting performance specifications. The paper also addresses concerns about false alarms and false replacements. The importance of using today's testability analysis tools for assessing and optimizing integrated vehicle health management systems is emphasized. With this technology, we could model a rocket engine test stand and utilize the existing test stand sensors as a baseline for testability analysis. We used the observed discrepancy maintenance reports provided by the test stand engineers to assign failure modes to the components.

Oldenkamp et al. [5] published a "Design of an Engine Test Stand: Design Report." The primary objective of this design project was to develop a test stand for a two-stroke model aircraft engine capable of measuring thrust and torque simultaneously and independently. This test stand was designed to help the University of Manitoba Aero Team obtain accurate performance data, leading to more successful outcomes in annual competitions. Previous studies, including patents and journal articles, measured thrust or torque. However, the proposed test stand utilizes a mechanism that enables the simultaneous and independent measurement of both quantities. This mechanism uses a two-piece test stand that decouples the effect of thrust and torque through a bearing shaft connected to the engine mounting plate. The quantities of interest will be autonomously measured using the conventional strain gauge-based contact method. Various alternative designs were considered during the concept development process. These designs were independently studied, and the final design was proposed through optimization based on the client's needs and specifications. Analytical modeling and several physical tests were conducted to assess the strength and effectiveness of the test stand. In conclusion, the study found that the proposed test stand, featuring robustness, portability, adaptability, and reliability, best suits the client’s needs and is a feasible and practical solution.

Tatarynow et al. [6] published an article titled "Test Stand for a Motor Vehicle Powered by Different Fuels" in Applied Sciences. This article discusses current testing methods for motor vehicle engines. Traction engines have traditionally been tested according to the WLTP (Worldwide Harmonized Light Vehicle Test Procedure) driving tests. Still, due to the “VW-gate” incident, these are now being supplemented by RDE (Real Driving Emissions) tests conducted under actual road conditions. The analysis of the state of knowledge and research directions to date indicates the need for the construction of a stand that allows for the testing of a complete vehicle admitted to traffic, testing of a motor vehicle with the possibility of simulating actual operating conditions, load setting with the ability to regulate it; feeding the engine with various fuels; modification of the software of controllers that have a direct impact on the control strategies of the engine, transmission, and traction control system; reading, recording, and analyzing the parameters of the operation of control systems in real-time; detailed recording and analysis of the combustion process occurring directly in the combustion chamber; and the measurement of emitted toxic substances.

Tests were conducted on a diesel motor vehicle bench with the above features, focusing on recording changes in combustion and injection process parameters. The tests were conducted under both static and dynamic conditions. Static tests were performed on a chassis dynamometer, involving the engine being indicated for different fuel dose control maps. The vehicle equipped with the test engine was driven at a constant speed on the chassis dynamometer and loaded with a drag force of 130 Nm. Dynamic tests were conducted under actual traffic conditions, but were limited to presenting results under static conditions. The main results of the tests are provided in the conclusion, which includes a general summary. Specifically, the results of the diesel tests demonstrate an attempt to adapt the engine to co-power with hydrogen.

Magryta et al. [7] published an article titled "FEM Simulation of Different Engine Mount Models in an Aircraft Piston Diesel Engine" in the journal Advances in Science and Technology. Research Journal. This article presents the results of numerical simulations using the Finite Element Method (FEM) to analyze the strength of engine mounts for an aircraft diesel engine

with opposed pistons, known as the PZL-100. Four versions of the mount, prepared by the aircraft engine manufacturer WSK "PZL-Kalisz," were analyzed. The tests were conducted using Catia v5 software within the Generative Structure Analysis module. The boundary conditions included the engine's gravity force, propeller thrust force, and propeller torque. S235JR steel was defined as the material. A design grid with tetrahedral elements and a single element size of 2 mm was used for the simulation. As part of the simulation study, four structural solutions for the test engine mounts were calculated based on strength. The results were compared, including the magnitude of stress maps and the deformation of the mount elements. Based on the obtained results, one of the mount versions was recommended for actual fabrication.

2 MATERIALS AND METHODS

This section examines the inventor's diesel engine test support structure model and analyses the diesel engine test support structure using the finite element method in Abaqus.

2.1. Modeling the Diesel Engine Test Support Structure in Inventor Software

Figure 1 shows the diesel engine test support structure, which was modeled based on the ISO 2768-mK standard and with the help of Autodesk Inventor software. This structure consists of nine members: a steel main frame, telescopic engine handle holders, a telescopic engine holder, a radiator holder, radiator axial arms, a battery holder, a fuel tank, engine handle axial arms, and a control panel holder.

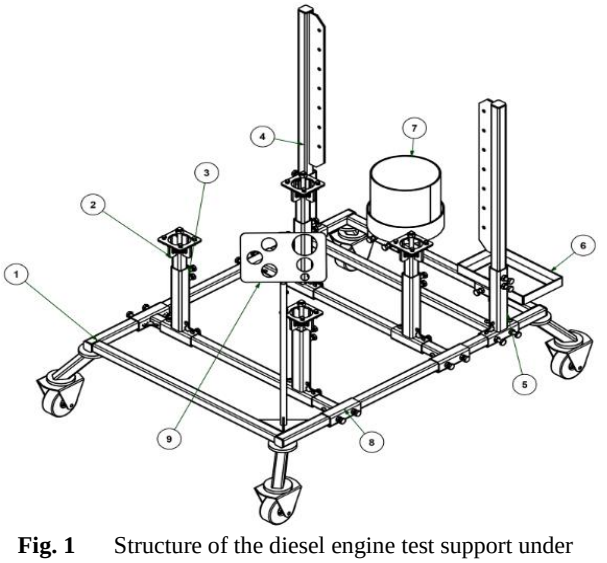

Fig. 1 Structure of the diesel engine test support under study: (a):1: Steel main frame, (b): 2: Telescopic engine handle holders, (c): 3: Telescopic engine holder, (d): 4: Radiator holder, (e): 5: Radiator axial arms, (f): 6: Battery holder, (g): 7: Fuel tank, (h): 8: Engine handle axial arms, and (i): 9: Control panel holder.

Figures 2(a) and 2(b) show the three-dimensional view of the Cummins model diesel engine test support structure and the side view of the structure in the inventor software, which is studied in this research. In the modeled structure, all parts are made of CK 45 medium carbon steel, commonly used to construct vehicle chassis and other high-strength automotive structures. The steel has a density of 7830 kg/m^3, a Poisson's ratio of 0.3, and a yield stress of 414 MPa, which is included in the mechanical analysis.

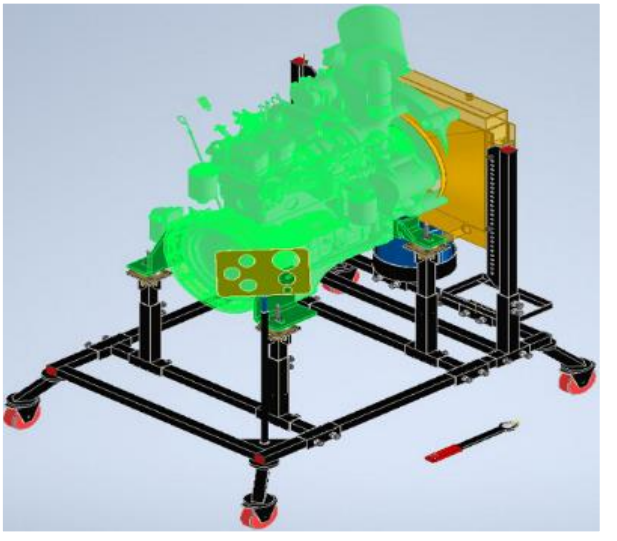

(a)

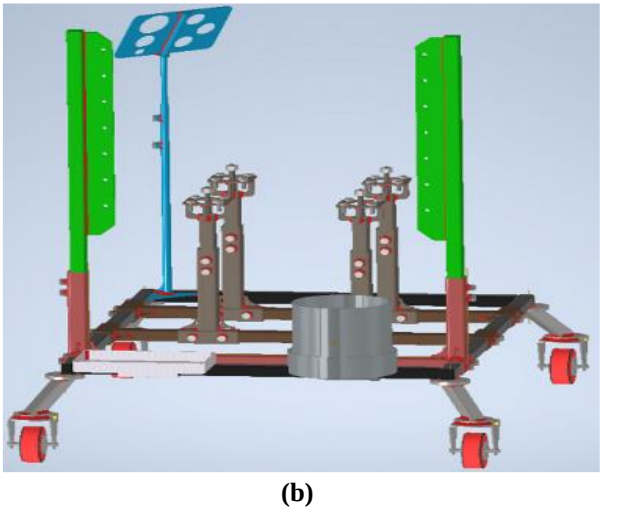

(b)

Fig. 2 (a): Three-dimensional view of the modeled diesel engine test support structure with the Cummins diesel engine model in Inventor software, and (b): Right side view of the modeled structure in Inventor software.

In the modeled structure, accurate measurements have been made of the dimensions of the actual structure, which include components: telescopic engine handle

holder, radiator holder, battery holder, fuel tank, control panel unit, steel frame, and connecting arms. "Table 1" shows the specifications of the diesel engine test components. All dimensions, weights, and thicknesses were measured in meters, kilograms, and millimeters, respectively. As mentioned earlier, CK 45 medium carbon steel was used due to its favourable mechanical properties. This type of sheet is considered due to its favourable properties, such as resistance to impact and heat, resistance to tension and friction, high strength, high welding, and machinability, as well as suitable elasticity and viscosity.

Table 1 Technical specifications of the modeled maintenance test engine diesel powered by Inventor Software

Part name	Dimensional specifications (m)	Weight (kg)	Quantity	Thickness (mm)	Materials
Frame	L1.3×0.04×0.04 L0.906×0.04×0.04	5.642 3.392	2 2	4 4	Ck45
Framework	0.906×1.3	30.235	1		Ck45
The final wheel	0.11×0.153	1	4	4	Ck45
Steel wheel	Ø0.04×Ø0.015×0.026	0.163	4		Ck45
Rubber wheel	Ø0.04×0.013		4		Rubber
Axle Wheel Industrial	Ø0.012×0.126	0.106	4		Ck45
Ball bearing roller	DIN-5405-T1 0.01×0.015×0.012		4	10	
Cotter Pin	DIN-6999 0.012×0.008		16		Ck45
The final maintenance structure	DIN-59410 0.04×0.04	0.723	4	4	Ck45
The heel	Ø0.1	0.740	8	12	Ck45
Telescopic-viewing motor	DIN-59410 L0.3×0.04×0.04	1.356	4	4	Ck45
Finger guard-motor	0.036×W 0.06L 0.033×W 0.06L	0.076 0.065	8 8	8 8	Ck45 Ck45
Page-maintainer-handle-motor	Ø0.081×L0.115×W0.11	0.331	4	6	Ck45
Engine Handle Rod	Ø0.015×L0.23	0.312	4		Ck45
Rear guard-radiator	DIN-59410 L1×0.04×0.04	4.522	2	4	Ck45
Plate-guard-radiator	L0.75×7×Ø0.012	2.367	2	6	Ck45
Telescopic observation	L0.897×W0.3	8.826	1		Ck45
Cap	0.04×0.04	0.061	6	5	Ck45
Battery holder	DIN-EN-10056 L0.19×0.04×0.04	0.173	2	4	Ck45
Battery maintenance	DIN-EN-10056 L0.32×0.04×0.04	0.291	2	4	Ck45
Wall Tank	L0.761×R0.119	5	1	4	Ck45
Maintenance tank	L0.836×W0.08×R0.131 Ø0.262	2.1 1.69	1 1	4 4	Ck45
Axis-dynamic	DIN-59410 L0.15×0.05×0.05×Ø2×0.014	0.657	12	3	Ck45
Control panel	DIN-EN-10060 Ø0.016×L0.6	0.954	1		Ck45
Advanced Control Panel	L0.03×W0.023 R0.015×R0.008	0.014	2	5	Ck45
Page Control Panel	L0.3×W0.02	1.386	1	4	Ck45
Axial Arm	L0.897×W0.15	5.761	2		Ck45
Reinforced telescopic and axial arms	L0.04×W0.04	0.028	25	٥٥	Ck45
Weight Total Construction Maintenance Diesel Engine Test Support Structure		232 kg			

2.2. Analysis of Diesel Engine Test Support Structure by Finite Element Method in Abaqus Software

In this section, the analysis of the diesel engine test support structure using the finite element method is conducted. Initially, the modeled structure is

transferred from Inventor Software to ABAQUS CAE 2018 Finite Element Software. In this analysis, as mentioned in the previous section, the structure is made of Steel CK 45, the specifications of which are presented in "Table 2".

Table 2 Mechanical properties of materials used in the structural maintenance test of the diesel engine in Abaqus software

Material	Density (kg/m^3)	Elastic modulus (MPa)	Poisson's ratio	Yield stress (MPa)
CK 45	7830	2.06×10^5	0.3	414

Static analysis is one of the critical parts of systems analysis, where displacements and stresses caused by static loads are calculated. Static analysis is divided into two categories: linear and non-linear. An analysis is called linear when non-linear phenomena such as plasticity, large deformations, large strains, creep, and other non-linear sources are not considered or their effects are applied linearly. Static loads refer to loads that do not change with time and are usually unaffected by damping.

The formulation of linear static problems in the form of matrix Equations to solve is Equation (1), where [K] is the rigidity matrix of the diesel engine test support structure, {U} is the displacement vector, and {F} is the force vector.

$$[K]\{U\} = \{F\} \tag{1}$$

In the Dynamic-Vibrational analysis and the calculation of the reliability coefficient for the diesel engine test support structure in non-elastic stress analysis, a mathematical Equation includes three principal stresses, known as the efficiency function. If the calculated yield function is greater than the initial value, the yield strength of the material, plastic strain, and softening or hardening will occur. In general, there are several yield functions to investigate the state of stress beyond the elastic region, including the von Mises stress criterion and the maximum shear stress. If a material is subjected to pressure beyond that, the yield surface changes in the elastic region. In this regard, there are two basic types of yield surface changes. One assumes that the center of the yield surface remains constant while, at the same time, the yield surface expands without deformation, which is known as isotropic hardening. Another case, kinematic hardening, assumes that the yield surface is visible in the stress space but does not change its size or shape. Both shear stress and von Mises stress are criteria used to predict the yield surface of flexible materials. In contrast, the maximum average stress criterion is commonly used to indicate the failure of brittle materials because the yield stress occurs at low-strain surfaces and is difficult to define. Shear and von Mises stress are generally used when structural materials are flexible. Von Mises' theory typically predicts failure more accurately, but Tresca's theory is often used in design because its use is more straightforward and more consistent. The Von Mises theory relates the distortion energy of a point under the general state of stress. A state of hydrostatic stress occurs when all three principal stresses are equal. In this condition, regular strains are equal in all directions, and there is no shear stress due to symmetry. The conventional design method in mechanical engineering, sometimes referred to as the classical method or deterministic design method, is based on the concept of the reliability factor. This means that different parts are designed so that the maximum applied stress is smaller than the minimum resistance of the materials used in the structure or part.

The von Mises stress for predicting failure in materials is calculated using Equation (2), where σ represents the everyday stresses, and τ represents the shear stresses.

$$\sigma_v = \sqrt{\frac{1}{2}\left[\left(\sigma_x-\sigma_y\right)^2+\left(\sigma_y-\sigma_z\right)^2+(\sigma_z-\sigma_x)^2+6(\tau_{xy}^2+\tau_{yz}^2+\tau_{zx}^2)\right]} \tag{2}$$

First state: In this static state, the effects of the weight of the parts on the four bases of the structure are assumed to be ideal. Figure 3 shows the relations of the equilibrium Equation analysis of the free body. P is the compressive force in this structure, and R_A and R_B are the reaction forces on cross-section A.

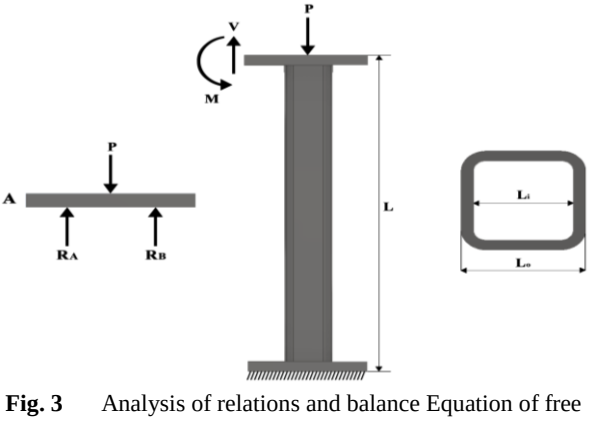

Fig. 3 Analysis of relations and balance Equation of free bodies.

The Factor of Safety (FOS) is a critical metric in evaluating the safety of structures and components under load. It indicates the ratio of the material's strength to the applied load and is defined as follows:

$$\text{FOS} = \frac{\sigma_y}{\sigma_{\text{applied}}} \quad (3)$$

Where σ_y is the yield stress of the material, and σ_{applied} is the applied stress. The closer the resulting value from the above Equation is to the desired value, the better the structure can ensure safety under the applied loads. The structure needs reinforcement or redesign if the FOS exceeds the desired value. This definition is in accordance with Eurocode 3 (EN 1993-1-1), Design of steel structures.

It is assumed that the side length of the square cross-section is equal to A. The area of the outer square is A^2, and the area of the inner square is B^2. Thus, the net cross-sectional area of the square in the structure is calculated using the following formula:

$$Area_{net} = Area_{outer} - Area_{inner} = A^2 - B^2 \quad (4)$$

If an axial force P is applied to the structure, then the axial stress σ is calculated as follows:

$$\sigma = \frac{P}{A_{net}} = \frac{P}{A^2 - B^2} \quad (5)$$

If a shear force V is applied to the structure, the shear stress τ in the square cross-section is calculated as follows:

$$\tau = \frac{V}{A_{net}} = \frac{V}{A^2 - B^2} \quad (6)$$

Suppose the bending moment and bending stress are applied to the structure.

In that case, they are calculated using Equation (7), where M is the bending moment, (I) is the Area moment of inertia of the square cross-section, σ is the bending stress, and Y is the distance from the neutral axis.

$$\sigma_b = \frac{M.Y}{I} = \frac{M.\frac{A}{2}}{\frac{1}{12}(A^4 - B^4)} = \frac{6M.A}{A^4 - B^4} \quad (7)$$

The displacement in a hollow section under an axial load P with length L, cross-sectional area A, and modulus of elasticity E is calculated as follows:

$$\delta = \frac{P.L}{A_{net}.E} = \frac{P.L}{(A^2 - B^2).E} \quad (8)$$

The natural frequency of a hollow section with a square cross-section and length L is calculated as follows:

$$f_n = \frac{1}{2\pi}\sqrt{\frac{k}{m}} \quad (9)$$

Where k is the stiffness of the system and m is the system's mass.

The second case: In this scenario, the dynamic and vibration loads caused by the diesel engine transferred to the structure are investigated. The goal is to determine a general Equation to explore the static vibrations of a beam. The adequate pressure P_{eff} is defined by the following Equation:

$$P_{eff} = -\frac{\partial^2\left[EI(x)\frac{\partial^2 \vartheta^s}{\partial x^2} + a_1\frac{\partial^3 \vartheta^s}{\partial x^2 \partial t}\right]}{\partial x^2} - m(x)\frac{\partial^2 \vartheta^s}{\partial t^2} - c\frac{\partial \vartheta^s}{\partial t} - \frac{\partial\left[N(x)\frac{\partial \vartheta^s}{\partial x}\right]}{\partial x} \quad (10)$$

In this formula, P_{eff} is the adequate pressure or force resulting from combining various forces and effects. The second derivative concerning the spatial variable x represents the bending or curvature in the structure. EI(x) is the bending stiffness or flexural rigidity, defined as a function of the spatial variable x, where E is the modulus of elasticity and I is the Area moment of inertia of the cross-section. ϑ^s represents the transverse displacement of the beam as a function of the spatial variable x and time t. The second derivative of displacement concerning the spatial variable x indicates the degree of bending at a specific point in the structure. a_1 is a coefficient multiplied by the third derivative of displacement with respect to the spatial variable x and time t, representing the time-dependent effects on deformation. m(x) is the mass per unit length, a function of the spatial variable x, multiplied by the second derivative of displacement with respect to time t, indicating the inertial forces. The damping coefficient c is multiplied by the first derivative of displacement about time t, representing the damping forces in the system. The axial force N(x), a function of the spatial variable x, is multiplied by the first derivative of displacement concerning x, then differentiated concerning x, representing the effect of axial forces on the structure. By combining these components, the formula for P_{eff} models the influence of all these forces and their impact on the structure, which can be used to analyze the dynamic and static behavior of the structure under various loading conditions.

2.2.1. Determining the Properties of Ingredients in The Property Module

"Table 2" shows the mechanical properties of CK 45 materials for the diesel engine test support structure, defined in the Abaqus software's property module. These properties include density, Poisson's ratio, modulus of elasticity, and yield stress (Figure 4).

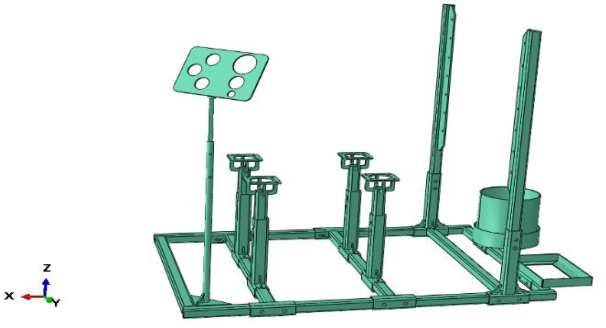

Fig. 4 Material property definition module in Abaqus software.

2.2.2. Assembling the Diesel Engine Test Support Structure in the Assembly Module

Each model in Abaqus may be composed of different parts that are used to put these parts together and form a final system, so by applying the assembly module; one can relate geometric constraints between them [20]. Figure 5 shows the assembled model of the structure prepared for diesel engine tests in Abaqus software. Additionally, in this Figure, the studied components are considered as the Body, which comprises six pieces in the Abaqus software environment.

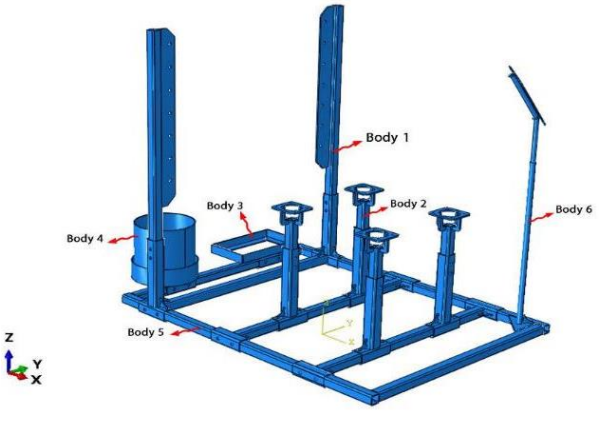

Fig. 5 The assembled structure model in the Assembly module and the examined components of the structure as a body in Abaqus software.

2.2.3. Determination of Analysis Specifications and Type of Solver in the Step Module in Abaqus Software

Every phenomenon in physics has a specific set of differential Equations. Choosing a suitable solver for model analysis is crucial, considering the static characteristics of the structure. The solver must be capable of performing static analysis of the model. In this regard, the STATIC GENERAL option in the Step module performs static analysis with a one-second interval. Additionally, the goal of using Abaqus software is to obtain and analyze output data [8]. For this purpose, the Step module is configured to display results related to stress, strain, displacement, and frequencies as output data at the end of the analysis.

2.2.4. Boundary Conditions and Load Application of The Structure in The Load Module in Abaqus Software

Figure 6 shows the boundary conditions and main forces applied to the entire diesel engine test support structure. These include the telescopic support of the engine handle, radiator and battery supports, tank, control panel plate steel frame, and axial arms implanted in the Abaqus software. In "Table 3", the number of concentrated forces on the structure, such as the battery, fuel tank, radiator, and engine bracket holders, is listed in Newtons, and suitable loading inputs are applied.

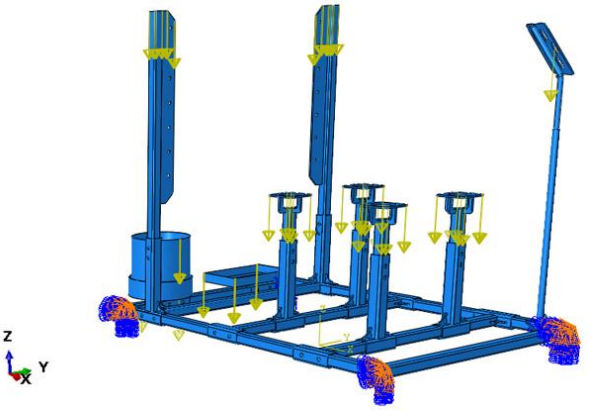

Fig. 6 Boundary conditions and structure support in the Load module in Abaqus.

Table 3 Compressive Loads Concentrated on the Structure

Parts	Compressive Load (N)	Parts	Compressive Load (N)
Battery holder	137.34	Reservoir holder	127.53
Control panel holder	23.2399	Engine handle holder	2452.5
Radiator holder	147.15		

2.2.5. Determining the Type of Structure Meshing in the Mesh Module in Abaqus Software

The mesh type and corresponding elements must first be specified to use the meshing module in Abaqus software. The elements have five unique characteristics that determine their behavior and meshing method.
These characteristics are divided into five main groups:

- Family

- Degrees of freedom
- Number of nodes
- Formulation method
- Integration method

Two types of pyramidal and cubical elements have been used to implement the structure from the Abacus software library. The quadratic tetrahedral element (C3D10) is a second-order 10-node tetrahedral pyramidal element. Additionally, the linear tetrahedral element (C3D4) is a three-dimensional element with 4 nodes and six-sided cubic elements [21]. The finite element mesh of the entire structure includes 30,894 elements and 62,662 nodes, as shown in [19]. In "Fig. 7", it can be seen that the number of mesh convergence elements (validation) of the diesel engine test holding structure has been equalized more accurately in 70000 finite elements, and according to this Figure, with the increase in the number of elements (the elements become finer), the stress has converged to a fixed limit [9].

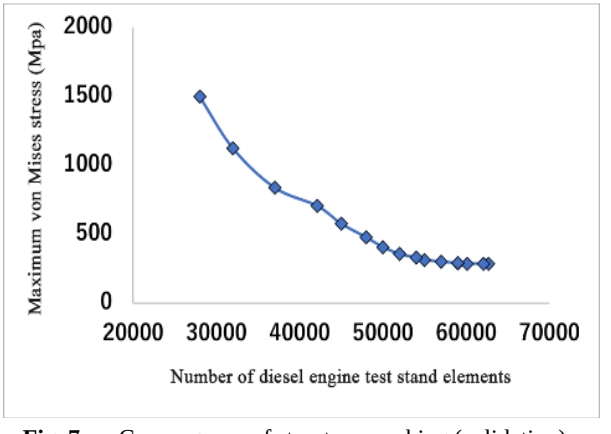

Fig. 7 Convergence of structure meshing (validation).

The closer we get to the number and areas of the maximum von Mises stress element, the lower the accuracy of the investigation [21]. Figure 8 shows the meshing module of the diesel engine test support structure in Abaqus software.

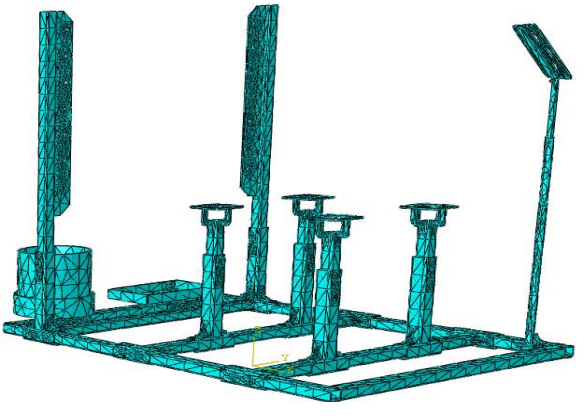

Fig. 8 Structure meshing in the Mesh module in Abaqus software.

3 RESULTS AND DISCUSSION

This section presents the results of the static analysis of the diesel engine test support structure and the modal analysis results of the diesel engine test support structure.

3.1. Results of Static Analysis of Diesel Engine Test Support Structure

Figure 9 shows the von Mises stress contour in megapascals. The highest von Mises stress occurred in the engine handle and its telescopic structure, ranging from 275 to 617 MPa. In contrast, the lowest von Mises stress was observed in the radiator plate holder and control panel assembly, with a value of approximately 100 MPa.

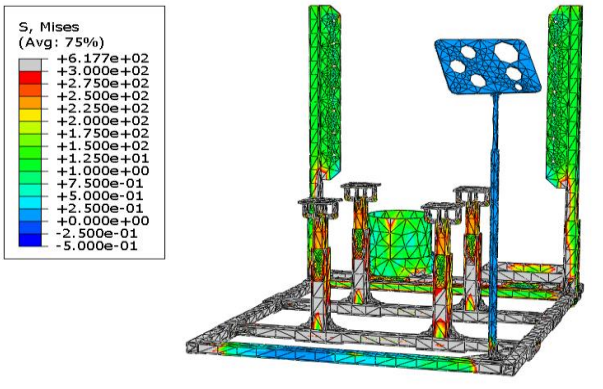

Fig. 9 Von Mises stress analysis contour of diesel engine test support structure.

Figure 10 shows the contour of the von Mises stress analysis path in the engine mounts. According to the contour results, the highest von Mises stress occurred in the range from the engine mounts to the supporting frame, between 250 and 300 MPa. Figure 11 shows the contour diagram of the von Mises stress analysis path for the engine handle holder. The initial stress at node 41504 is approximately 200 MPa, and the path first descends until it reaches the second node 28733. From there, the stress increases until it reaches the third node, 4490, then decreases again. The maximum stress at the third node is approximately 300 MPa.

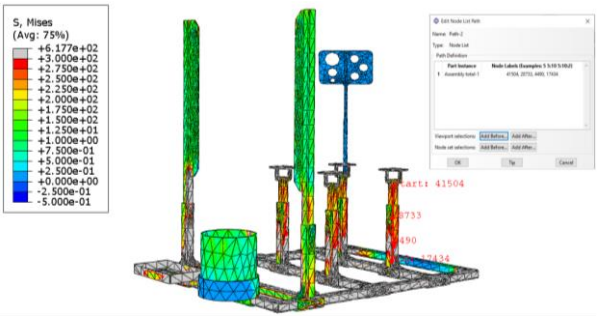

Fig. 10 The contour of von Mises stress analysis path in the category of structural engines.

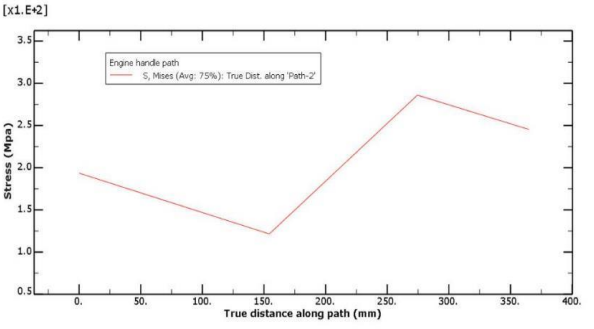

Fig. 11 Contour diagram of von Mises stress analysis path in the engine handle holder.

In "Fig. 12", the displacement contour of the structure is shown. According to these results, the most significant displacements occurred in the holders and radiator plates, ranging from 1.204 to 1.685 mm. The minor displacement occurred in the battery holder, control panel holder, and structural frame in the y direction, ranging from 0.2408 to 0.9630 mm.

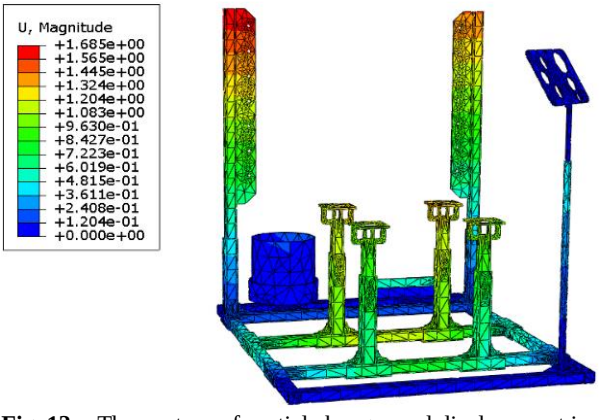

Fig. 12 The contour of spatial changes and displacement in the diesel engine test support structure.

Figure 13 shows the shear stress contour in the XY direction of the structure (S12). The highest shear stress occurred in the telescopic areas, radiator plates, part of the fuel tank, part of the battery holder, and the transverse frame of the structure, with values ranging from 16.0 to 68.2 MPa. The lowest shear stress occurred in the longitudinal frame, a control panel holder, the outer frame of the battery holder, and part of the fuel tank.

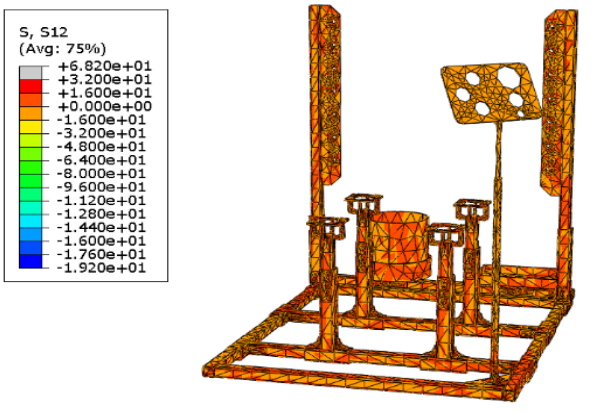

Fig. 13 Shear stress contour in the XY direction (S12) in the diesel engine test support structure.

3.2. Results of Modal Analysis of Diesel Engine Test Support Structure

In the modal analysis of the diesel engine test support structure, vibration amplitudes resulting from engine start-up and vibrations were observed. As shown in "Figs. 14(a) & 14(b)", mode one occurred at a frequency of 1.87 Hz with a displacement of 0.05562 mm related to the radiator support, and mode two occurred at a frequency of 7.20 Hz with a displacement of 0.08135 mm related to the engine handles near the radiator.

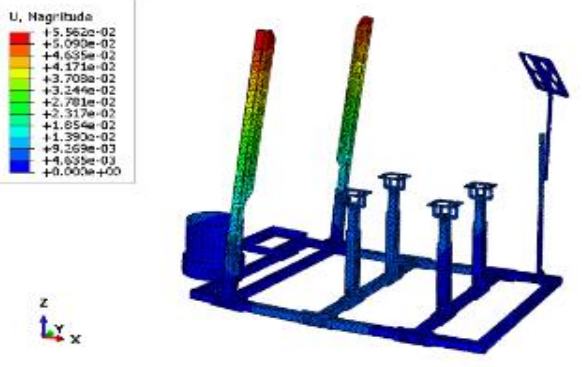

(a)

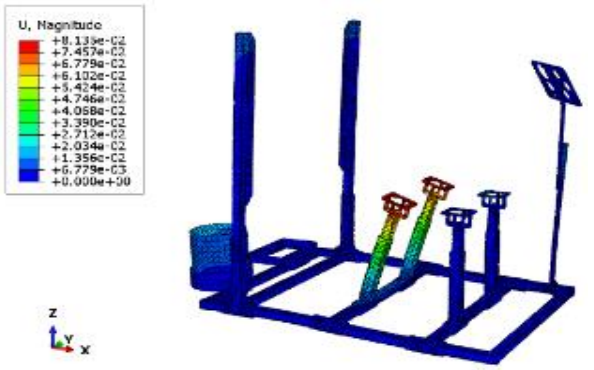

(b)

Fig. 14 (a): First mode, and (b): Second mode in the modal analysis of the diesel engine test support structure due to engine vibrations.

In “Figs. 15(a) & 15(b)”, mode three and mode four, respectively, occurred at a frequency of 8.36 Hz with a displacement of 0.07429 mm related to the engine handles and fuel tank and at a frequency of 9.45 Hz with a displacement of 0.05419 mm related to the engine handles, two longitudinal beams of the structure's floor, the fuel tank, and the control panel holder. Figures 16(a) and 16(b), for mode five and mode six, respectively, show a frequency of 10 Hz with a displacement of 0.05573 mm related to the engine handles and two transverse beams of the structure's floor and a frequency of 11 Hz with a displacement of 0.05659 mm related to the battery holder, fuel tank, engine handles, and two transverse beams of the structure's floor. Table 4 shows the frequency values in Hz, displacement values in mm, and the corresponding modes [10].

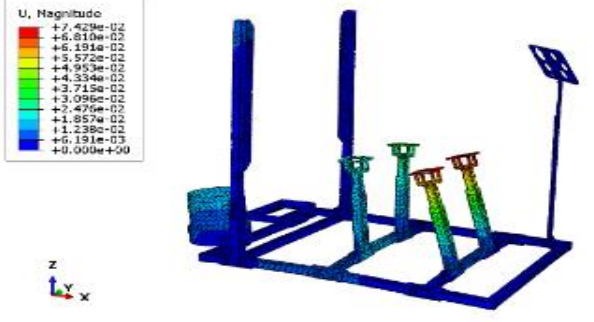

(a)

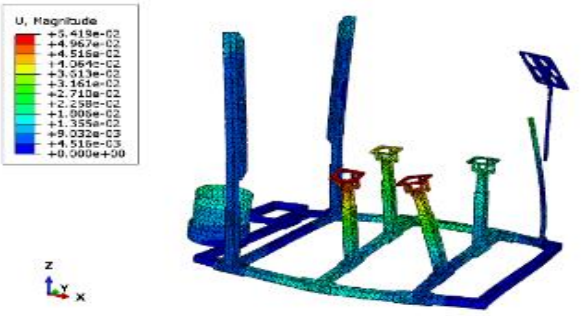

(b)

Fig. 15 (a): Third mode, and (b): Fourth mode in the modal analysis of the diesel engine test support structure due to engine vibrations.

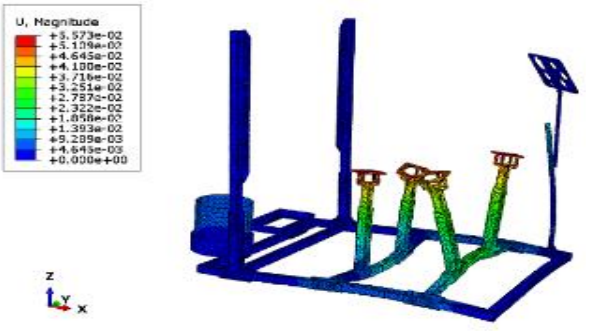

(a)

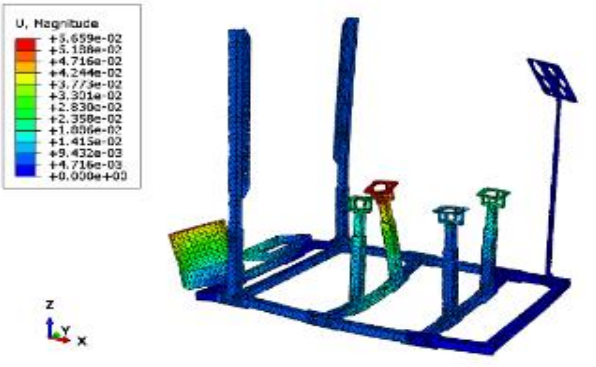

(b)

Fig. 16 (a): Fifth mode, and (b): Sixth mode in the modal analysis of the diesel engine test support structure due to engine vibrations.

Table 4 Frequency value in Hertz and Displacement value of different members

Member No.	Mode No.	Displacement value (mm)	Frequency (HZ)	Member No.	Mode No.	Displacement value (mm)	Frequency (HZ)
Member 1	First	0.05562	1.87	Member 4	Fourth	0.05419	9.45

Member 2	Second	0.08135	7.20	Member 5	Fifth	0.05573	10
Member 3	Third	0.07429	8.36	Member 6	Sixth	0.05659	11

3.2.1. Transverse Vibrations Due to Engine Dynamics in the Diesel Engine Test Support Structure

Transverse vibrations, resulting from engine dynamics and vibrations, are transmitted to the structural members. These values vary depending on displacement and time for each structure's members. The amplitude of the waves in the dynamic-vibrational analysis of the engine to the structure is defined as sinusoidal (Sin). Figure 17 shows the Time/Frequency and Amplitude/Displacement diagram. The displacement (U) values in millimeters and time (T) in seconds were extracted based on XY data and the analysis of the structure's vibration outputs. The structure's natural frequencies, forces, and modes were analyzed using the frequency solver in Abaqus software with the Lanczos method [11].

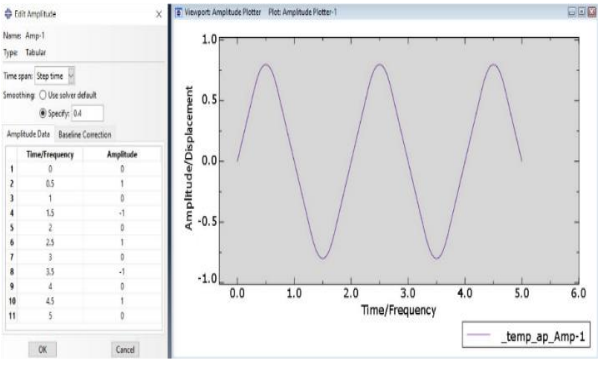

Fig. 17 Time/Frequency and Amplitude/Displacement Diagram: Sinusoidal wave amplitude in Abaqus software.

3.2.2. Transverse Vibrations of Member 1 (Radiator Holder)

Figure 18 shows the displacement contour of the radiator holder resulting from the engine's dynamics and vibrations. According to these results, the maximum displacement of 0.6350 µm and the minimum displacement of 0.05291 µm occurred periodically over 45 seconds with sinusoidal waves. In "Fig. 19", the maximum displacement of 0.1 mm was observed at the 37th, 32nd, and 17th seconds. The minimum displacement of -0.1 mm occurred at the 6th, 20th, 27th, and 40th seconds.

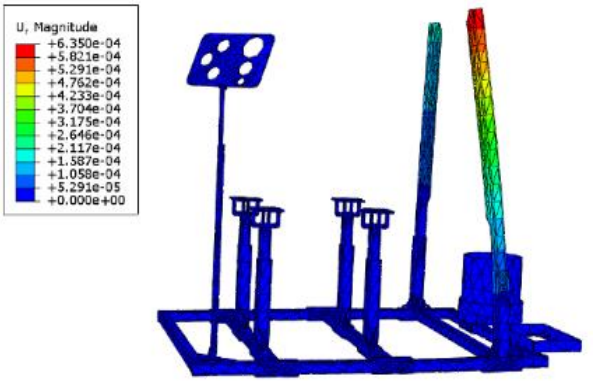

Fig. 18 Displacement contour of radiator holder member one due to engine dynamics.

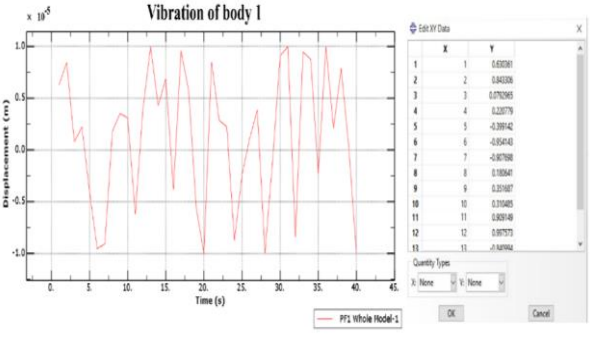

Fig. 19 Transverse vibration of radiator holder member one due to engine dynamics.

3.2.3. Transverse Vibrations of Member 2 (Motor Handle Holder)

Figure 20 illustrates the displacement contour of the motor handle holder resulting from engine dynamics and vibrations. According to these results, the maximum displacement of 0.5446 µm and the minimum displacement of 0.04538 µm occurred periodically over 45 seconds with sinusoidal waves. In "Fig. 21", the maximum displacement of 0.1 mm was observed at the 3rd, 11th, 18th, 30th, and 31st seconds. The minimum displacement in the -0.05 to -0.1 mm range occurred at the 7th, 18th, and 22nd seconds.

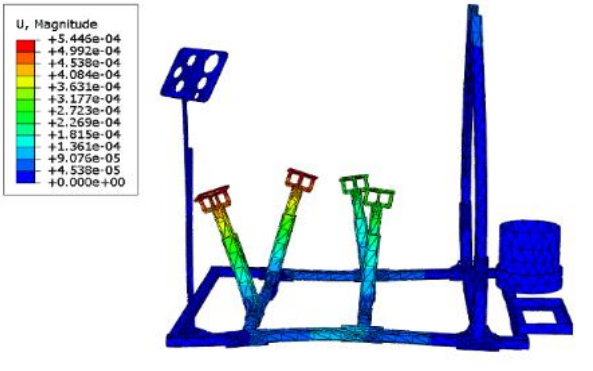

Fig. 20 Displacement contour of motor handle holder member two due to engine dynamics.

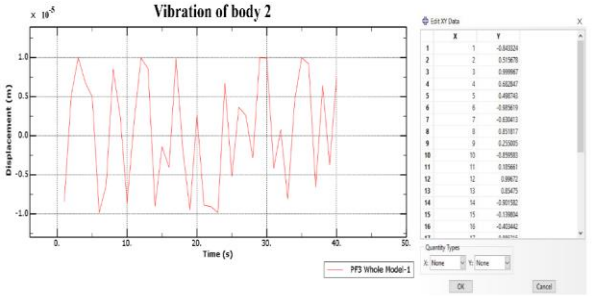

Fig. 21 Transverse vibration of motor handle holder member two due to engine dynamics.

3.2.4. Transverse Vibrations of Member 3 (Battery Holder)

Figure 22 illustrates the displacement contour of the battery holder resulting from engine dynamics and vibrations. According to these results, the maximum displacement of 1.134 μm and the minimum displacement of 0.0945 μm occurred periodically over 45 seconds with sinusoidal waves. In "Fig. 23", the maximum displacement of 0.1 mm occurred at the 7th, 10th, 12th, and 32nd seconds. The minimum displacement of -0.1 mm happened at the 2nd, 4th, 11th, 14th, 25th, 28th, and 35th seconds.

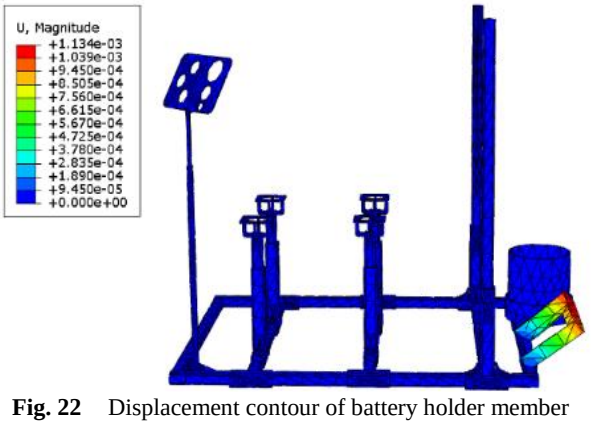

Fig. 22 Displacement contour of battery holder member three due to engine dynamics.

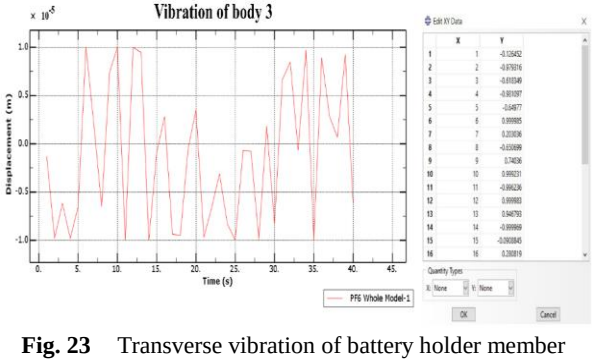

Fig. 23 Transverse vibration of battery holder member three due to engine dynamics.

3.2.5. Transverse Vibrations of Member 4 (Fuel Tank)

Figure 24 shows the displacement contour of the fuel tank resulting from engine dynamics and vibrations. According to these results, the maximum displacement of 0.5750 μm and the minimum displacement of 0.04791 μm occurred periodically over 45 seconds with sinusoidal waves. In "Fig. 25", the maximum displacement of 0.1 mm occurred at the 4th, 25th, and 30th seconds. The minimum displacement in the -0.05 to -0.1 mm range happened at the 6th, 8th, 14th, 29th, and 32nd seconds.

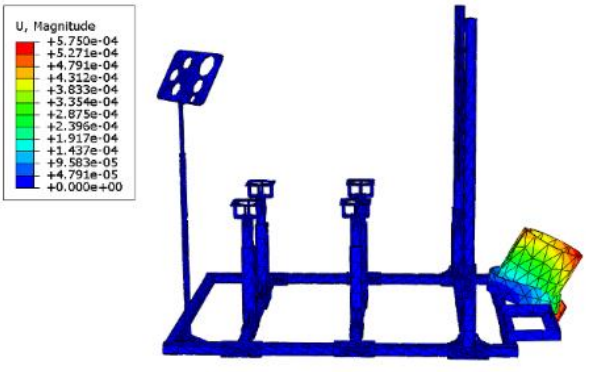

Fig. 24 24 Displacement contour of fuel tank member four due to engine dynamics.

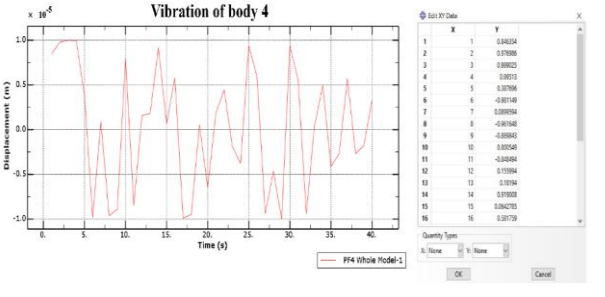

Fig. 25 Fuel tank member four transverse vibration due to engine dynamics.

3.3. Factor of Safety (FOS)

"Table 5" presents the safety factors of various diesel engine test stand structure components under critical conditions. The safety factor for the principal longitudinal and transverse support frames (Body 5) is the lowest in the structure (0.67), indicating that this part requires reinforcement. Additionally, the safety factors for the battery support frame (Body 3), radiator support frame (Body 1), engine mount support frame (Body 2), fuel tank support frame (Body 4), and control panel assembly support frame (Body 6) are the highest in the structure (ranging from 1.38 to 2.76), suggesting that these parts are safe and do not require reinforcement. Therefore, based on standard safety factor studies used in engineering structures, [16] we

recommend applying a safety factor range of 1.5 to 3 for unsafe and critical areas under high stress.

Table 5 The safety factor of different parts of the diesel engine test support structure under critical conditions

Selected region on the frame	Von-Mises stress (MPa)	Factor of Safety (FOS)	Critical Point	Ultimate Strength (MPa)
Body 1 (Fig.6)	175.0	2.36	No	413.0
Body 2 (Fig.6)	300.0	1.38	No	414.0
Body 3 (Fig.6)	225.0	1.84	No	414.0
Body 4 (Fig.6)	150.0	2.76	No	414.0
Body 5 (Fig.6)	617.7	0.67	Yes	413.859
Body 6 (Fig.6)	12.50	33.12	No	414.0

3.4. Results of Fracture Analysis, Fatigue Life, Crack Growth Modal, Buckling, and Bending Test in the Structure

Fatigue is one of the leading causes of failures in mechanical and structural systems. Fatigue life is the total number of loading cycles required to initiate a fatigue crack and the number of cycles needed for the crack to propagate before sudden failure occurs. Since the analytical determination of fatigue crack propagation life in actual geometries is rarely feasible, crack propagation problems are usually solved using computational methods. In this review, the use of the Finite Element Method (FEM) and the Extended Finite Element Method (XFEM) for modeling fatigue crack propagation is discussed [12].

3.4.1. Using XFEM in Fracture Mechanics Analysis

The XFEM (Extended Finite Element Method) is an advanced technique in fracture mechanics analysis used for modeling cracks and discontinuities in structures without needing to re-mesh the geometry. In XFEM, cracks are implicitly modeled within the displacement field, and enriched shape functions represent displacement discontinuities. This method allows for more accurate modeling of crack growth and prediction of its path, as it does not require changes to the mesh structure during the analysis. XFEM uses level set and enrichment functions to represent cracks and discontinuities, enhancing precision and efficiency in analyzing complex fracture problems [13]. This study section presents the results obtained from analyses using the advanced XFEM in the Abaqus finite element software. These results include fracture mechanics, crack growth, and fatigue analyses in the diesel engine test support structure.

3.4.1.1. XFEM Analysis Results, Static and Dynamic Analysis

The geometry, dimensions, and boundary conditions are shown in “Fig. 26(a)”.

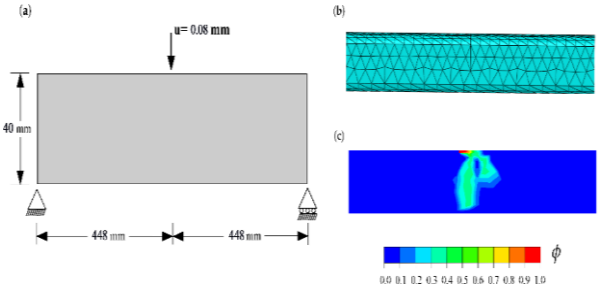

Fig. 26 Three-point bending test: (a): geometry, dimensions, and boundary conditions, (b): finite element mesh, and (c): phase field contour at the end of the analysis.

A vertical displacement of 0.08 mm is applied at the top of the beam at a horizontal distance of 448 mm from each support. No initial crack is defined in the beam. The mechanical behavior of the beam is characterized by Young's modulus of E =100 MPa and a Poisson's ratio of ν = 0. 1. It is noted that in the model, the material strength is explicitly incorporated into the structural response. As a result, the outcomes are largely insensitive to the phase field length scale choice, which is assumed to be ℓ = 0.5 mm here. The model is meshed using 10-node quadratic tetrahedral elements (C3D10 in Abaqus). As shown in “Fig. 26(b)”, the mesh is refined in the center of the beam, where the crack is expected to nucleate and grow. The characteristic element size is at least five times smaller than the phase field length scale, and the total number of elements is 18970. The results are computed using the monolithic scheme. The static analysis results indicate stress concentrations near the connections of the structure to the motor and the bases. Figure 26(a) shows the geometric model of the structure with specified loading, while “Fig. 26(b)” displays the finite element mesh. Figure 26(c) illustrates the stress distribution results after the load is applied. The dynamic analyses also examine the structure's response to variable loads and show how the structure behaves under dynamic loading. These analyses indicate that the critical stress points and discontinuities are primarily located in the middle of the connections to the motor and between the bases [14-15].

3.4.2. Modal Analysis of Crack Growth in Structure

The following images show the modal shapes of different cracks obtained using XFEM. These images depict the crack paths and displacement discontinuities in each mode. Figure 27 displays both (a) the front and (b) rear views of cracks in various modes. Modal analysis helps identify the crack patterns and the

behavior of different crack modes, illustrating how the cracks propagate within the structure.

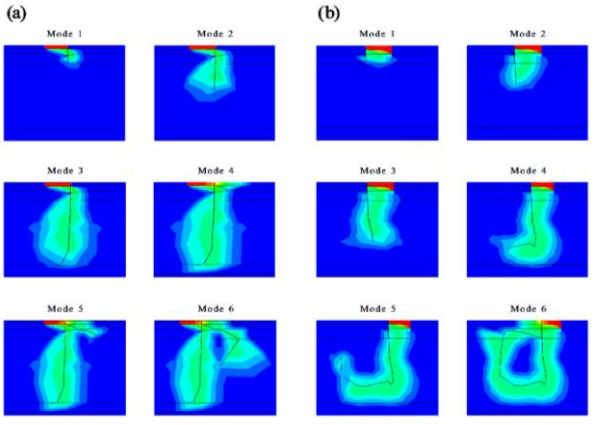

Fig. 27 Modal analysis of cracks: (a): front view with various crack modes, and (b): rear view with various crack modes.

3.4.3. Fatigue Life and Crack Growth Analysis in Structure

Figure 28 illustrates the fatigue life and crack growth analysis of the structure under dynamic loading.

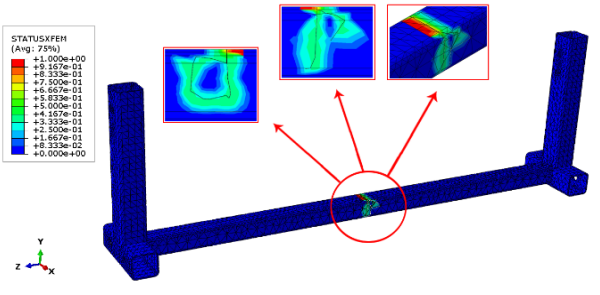

Fig. 28 Fatigue life and crack growth analysis of the structure under dynamic loading.

These analyses indicate that the critical crack points are located near the connections of the structure to the motor and the bases. By examining the gradual changes in the crack and the effects of cyclic loads, a better understanding of the structure's lifespan and weak points can be achieved. The highest stress occurs in the upper regions of the structure. Additionally, the lowest stress is observed in the middle and lower areas of the structure, indicating weakness and the application of excessive load in the upper regions of the structure. Fatigue and crack growth analysis help identify potential crack paths and critical areas, enabling necessary actions for design improvement, increased durability, and optimization. The numerical values indicate the crack status in the model elements. A value of 1.0 signifies a fully developed crack and the highest level of crack and discontinuity in the XFEM model within the structure. Conversely, a value of 0.0 indicates no crack and the lowest level of crack and discontinuity in the structure.

Fatigue analysis under cyclic loading, as shown in “Fig. 29”, represents the variations in the applied force relative to the number of loading cycles.

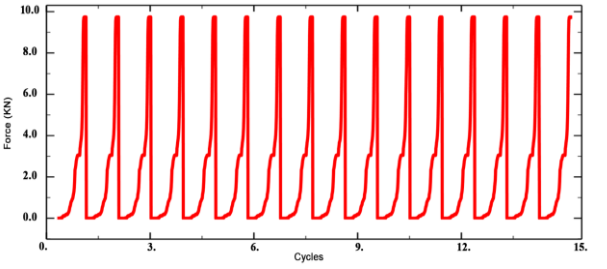

Fig. 29 The diagram of applied force variations concerning the number of loading cycles in the fatigue analysis of the diesel engine test support structure.

This diagram illustrates the dynamic behavior of the component under cyclic loading, where the applied force varies between 0 and 10 KN over 15 cycles. Each cycle represents a complete period of loading and unloading the force from the component. Therefore, this force-cycle diagram can accurately predict the component's useful life in the diesel engine test support structure. The results indicate stable cyclic loading behavior and its impact on the component's fatigue life. Analyzing the data, the component's fatigue life was predicted, and critical points that could lead to failure were identified.

3.4.4. Force-Displacement Relationship

Figure 30 shows the Force-Displacement diagram, illustrating the changes in applied force with crack displacement.

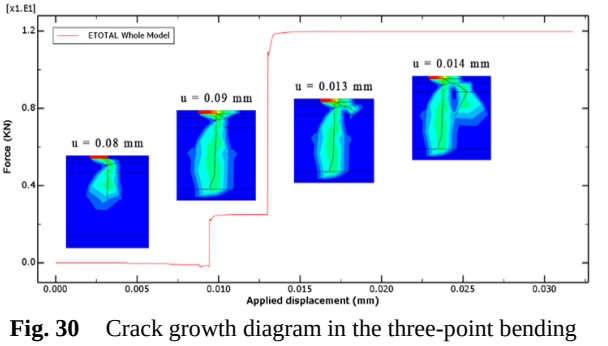

Fig. 30 Crack growth diagram in the three-point bending test: force response versus displacement.

As expected and consistent with the results obtained by reference [13], a crack nucleates at the bottom of the beam, at the center of the beam axis. The crack propagates directly upwards until it reaches the top, as shown in “Fig. 26(c)”. The force response versus displacement closely agrees with the predictions of reference [13]. This diagram aids in a more detailed

analysis of crack behavior and in predicting the structure's fatigue life. By analyzing the force-displacement diagram, it is possible to identify points where the crack rapidly proliferates and sudden changes in the structure's behavior occur. This information can be used to design a more robust structure and optimize maintenance and repair processes. The highest displacement and crack growth, corresponding to the late stages of crack propagation, is 0.014 mm with a force of 12 KN in the structure. Additionally, the lowest displacement and crack growth, corresponding to the early stages of crack initiation, is 0.08 mm with a force of 2 KN in the structure. These results indicate stability and weakness in the structure, respectively.

3.4.5. Buckling Mode Analysis and Critical Load Calculation in the Structure

In this section, the buckling mode analysis for the diesel engine test support structure was conducted, and the critical loads for each mode were calculated. This analysis was performed using Abaqus software, which selected the subspace solver for its high efficiency and accuracy in analyzing linear buckling problems. This solver facilitates the accurate determination of eigenvalues and critical buckling modes, which are crucial for assessing the stability of structures under compressive loads.

Table 6 Buckling Mode Shapes of the Engine Mount in the Diesel Engine Test Support Structure

1st Mode	2nd Mode	3rd Mode	4th Mode	5th Mode
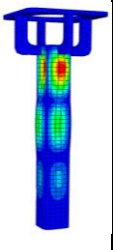	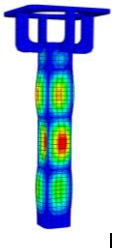	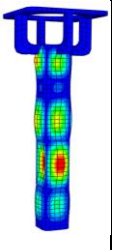	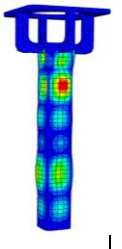	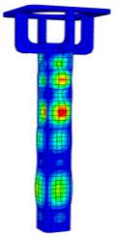
6th Mode	**7th Mode**	**8th Mode**	**9th Mode**	**10th Mode**
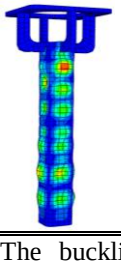	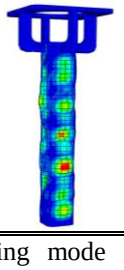	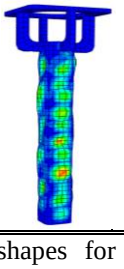	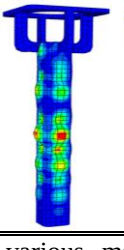	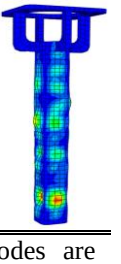

The buckling mode shapes for various modes are presented in "Table 6", illustrating the distribution of stresses and critical areas in each buckling mode. Eigenvalues for ten different buckling modes were obtained, representing the factors by which the initial load must be multiplied to determine the critical buckling load for each mode. This analysis applied an initial load of 613 N (for one engine mount) as a concentrated force at specific structure points. Subsequently, the critical buckling load for each mode was calculated using these eigenvalues. The critical buckling load is the load at which the structure becomes unstable under compressive forces, typically considered a key indicator in structural design to prevent sudden failure [17].

The computational results are presented in "Table 7", showing the critical buckling loads versus mode numbers. The results indicate that the critical buckling load varies significantly across different modes, highlighting the need for more precise structural design to prevent buckling under critical conditions.

Table 7 Eigenvalues and Calculated Critical Buckling Loads for the First 10 Buckling Modes

Mode No.	Eigenvalue	Critical Load (KN)
First	740.35	453.94
Second	804.32	493.05
Third	835.09	511.41
Fourth	898.73	550.96
Fifth	934.02	572.52
Sixth	981.22	601.79
Seventh	1062.2	651.11
Eighth	1074.9	658.91
Ninth	1022.6	627.84
Tenth	1056.0	647.93

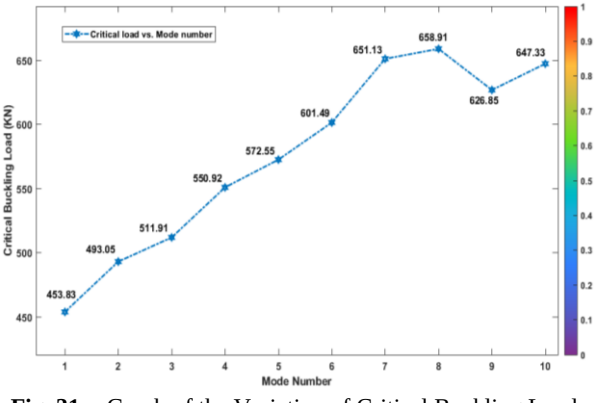

Fig. 31 Graph of the Variation of Critical Buckling Load concerning Mode Number.

Figure 31 graphically displays the variation of essential buckling loads with respect to the mode numbers. The first and second modes, with eigenvalues of 740.35 and 804.32, respectively, are particularly significant due to their greater impact on the structure's overall stability. Therefore, these modes should be a primary

consideration in the final design decision-making process.

Ultimately, this analysis demonstrates that the critical buckling load for all modes is significantly higher than the initial load applied to the structure, indicating that the structure is safe against the current loads. However, to enhance safety margins and ensure the structure's stability under unexpected or critical conditions, it is recommended that higher safety factors be incorporated into the final design. Specifically, it is suggested that the critical buckling load be considered 1.5 to 2 times the calculated value. Additionally, reviewing and reinforcing the sensitive and vital areas of the structure can prevent buckling under critical conditions and ensure overall structural safety.

3.4.6. Stress Distribution and Safety Assessment of the Axial Arm under Three-Point Bending

This section examines the Von Mises stress distribution in the axial arm supporting the engine mounts under three-point bending loading. Figure 32 illustrates the Von Mises stress distribution in the axial arm.

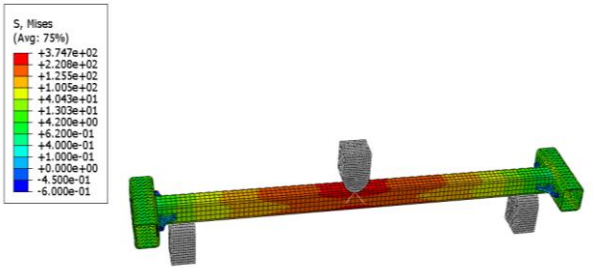

Fig. 32 Von Mises stress distribution in the axial arm supporting the engine mounts under a three-point bending load.

The maximum Von Mises stress, recorded at 374.7 MPa, is located in the central region of the beam, directly beneath the point of concentrated load application. This area experiences the highest bending stress due to its position at the peak of the bending moment. Conversely, the minimum Von Mises stress, which is 13 MPa, is observed in regions farther from the center of the beam and closer to the supports.

Considering the three-point bending test and similar loading conditions for the engine mounts installed on this axial arm, the analysis results indicate that the beam possesses sufficient safety margins. Compared to the material's yield stress and operational conditions, the maximum stress within the structure remains within a range that ensures the structure's resistance to the applied loads, thus preventing failure or yielding under normal operating conditions [18]. This assessment demonstrates that, although the center of the beam bears the highest stress, the overall structure effectively withstands the applied loads. The design and safety evaluation confirm the beam's ability to withstand both dynamic and static loads. Therefore, it can be concluded that the beam used for installing the engine mounts is safe under normal operating conditions.

4 CONCLUSIONS

In this study, a comprehensive analysis of the Static, Modal vibration, Safety factor, Fatigue life, and Modal crack growth characteristics of the diesel engine test support structure (ETSS) was conducted using Finite Element Method (FEM) and Extended Finite Element Method (XFEM). The primary objective of this research was to evaluate the structure’s performance, identify critical stress and vibration points, and predict fatigue life to enhance safety, reinforce, and optimize the support structure.

The findings can be summarized as follows:

- The static analysis revealed that the maximum von Mises stress ranged between 275 and 617 MPa in the telescopic supports of the engine handle and the longitudinal and transverse frames. The minimum stress values were observed in the radiator holders, fuel tank, and control panel. The stress path analysis also indicated that critical stress points are concentrated in the moving parts and base supports, which require reinforcement.
- The displacement and stress path analysis further revealed that the maximum displacements ranged between 1.204 and 1.685 mm in the radiator holders. In contrast, the most minor displacements occurred in the battery holders and control panel, ranging from 0.2408 to 0.9630 mm. These findings underscore the need to reinforce areas subjected to large loads.
- The shear stress analysis in different directions (XY, XZ, YZ) indicated that the highest stress occurred in the telescopic areas, radiator plates, and parts of the fuel tank and battery holders. These areas require special attention in design and reinforcement.
- The analysis of lateral vibrations caused by the engine's dynamics revealed that these vibrations are transmitted to the structure’s components and vary for each structural member depending on displacement and time. Modal analysis showed that the maximum displacement observed was 0.08135 mm at a frequency of 7.20 Hz. These vibrations could lead to damage over time, necessitating proper management and control.
- The fatigue and crack growth analysis using XFEM results indicated that the maximum crack growth was 0.014 mm under a force of 12 KN, predominantly in critical areas such as motor connections and base supports. These findings highlight the need for monitoring and reinforcing vulnerable areas to prevent fatigue-induced failures.

- The safety factor analysis revealed that while most structural parts have sufficient safety margins, the central longitudinal and transverse support frames require reinforcement. It is recommended to use a safety factor between 1.5 and 3 for high-stress areas to ensure the overall structural safety.
- The buckling analysis results for the engine mount structure showed that the structure is safe under the current applied loads, as the critical buckling loads are significantly higher than the initial load of 613 N. The first and second modes, with eigenvalues of 740.35 and 804.32, have a more significant impact on the stability of the structure and should be prioritized in the final design. To enhance safety and ensure the structure's strength under critical conditions, it is recommended to incorporate a safety factor of 1.5 to 2 times in the final design and reinforce sensitive areas.
- The results of the three-point bending test on the axial arm supporting the engine mounts showed that the maximum Von Mises stress, measured at 374.7 MPa, is located in the central region of the beam, directly beneath the point of concentrated load application. However, the minimum Von Mises stress, recorded at 13 MPa, was observed in areas farther from the center of the beam and closer to the supports. This analysis demonstrated that the axial arm has sufficient safety margins and is resistant to the applied loads, particularly under normal operating conditions. Therefore, the design and safety evaluation confirm that this arm can withstand dynamic and static loads and is adequately safe.

Future research could build upon the present findings by conducting experimental validation through full-scale prototype testing and sensor-based data acquisition. Moreover, investigating the structural performance under multi-axial and time-dependent loading conditions—such as thermal fluctuations, impact, and cyclic fatigue—may yield deeper insights into long-term durability. Exploring material optimization techniques and implementing multi-objective design strategies could further enhance structural efficiency, resilience, and cost-effectiveness.

REFERENCES

[1] Koch, L., Zeller, P., Test Stand for Dynamic Investigations of Combustion Engines, Automobiltech. Z., (Germany, Federal Republic of) Vol. 89, No. 11, 1987.

[2] Von Thun, H. J., A New Dynamic Combustion Engine Test Stand with Real-Time Simulation of The Vehicle Drive Line, SAE Transactions, Jan 1, 1987, pp. 385-91.

[3] Voigt, K. U., A Control Scheme for A Dynamical Combustion Engine Test Stand, InInternational Conference on Control 1991, Control'91, IET, Vol. 25, 1991, pp. 938-943.

[4] Temple, G., Jize, N., and Wysocki, P., Testability Modeling and Analysis of a Rocket Engine Test Stand, In 2005 IEEE Aerospace Conference, 2005, pp. 3874-3895.

[5] Oldenkamp, A., Omid, B., Skene-Hamilton, C., and Egilson, K., Design of an Engine Test Stand: Design Report, 2012.

[6] Tatarynow, D., Longwic, R., Sander, P., Zieliński, Ł., Trojgo, M., Lotko, W., and Lonkwic, P., Test Stand for a Motor Vehicle Powered by Different Fuels. Applied Sciences, Vol. 12, No. 20, 2022, pp. 10683.

[7] Magryta, P., Pietrykowski, K., and Borowiec, P., FEM Simulation of Different Engine Mount Models in an Aircraft Piston Diesel Engine. Advances in Science and Technology, Research Journal, Vol. 16, No. 5, 2022.

[8] Gholami, N., Afsari, A., Nazemosadat, S. M., and Afsari, M. J., Simulation and Dynamic-Thermal Analysis of Ceramic Disc and Brake Pad for Optimization by Finite Element Method, International Journal of Advanced Design & Manufacturing Technology, Vol. 16, No. 4, 2023.

[9] Nazemosadat, S. M., Ghanbarian, D., Naderi-Boldaji, M., and Nematollahi, M. A., Structural Analysis of a Mounted Moldboard Plow Using the Finite Element Simulation Method, Spanish Journal of Agricultural Research, Vol. 20, No. 2, 2022, pp. e0204-, https://doi.org/10.5424/sjar/2022202-18157.

[10] Reynders, E., System Identification Methods for (Operational) Modal Analysis: Review and Comparison, Archives of Computational Methods in Engineering, Vol. 19, 2012, pp. 51-124.

[11] Khennane, A., Introduction to Finite Element Analysis Using MATLAB® and abaqus, CRC Press, 2013.

[12] Rege, K., Lemu, H. G., A Review of Fatigue Crack Propagation Modelling Techniques Using FEM and XFEM, InIOP Conference Series: Materials Science and Engineering, IOP Publishing, Vol. 276, No. 1, 2017. pp. 012027.

[13] Wells, G. N., Sluys, L., A New Method for Modelling Cohesive Cracks Using Finite Elements, International Journal for Numerical Methods in Engineering, Vol. 50, No. 12, 2001, pp. 2667-82.

[14] Wu, J. Y., A Unified Phase-Field Theory for The Mechanics of Damage and Quasi-Brittle Failure, Journal of the Mechanics and Physics of Solids, Vol. 103, 2017, pp. 72-99.

[15] Wu, J. Y., Nguyen, V. P., A Length Scale Insensitive Phase-Field Damage Model for Brittle Fracture, Journal of the Mechanics and Physics of Solids, Vol. 119, 2018, pp. 20-42.

[16] Burr, A., Cheatham, J., Mechanical Design and Analysis, 2nd ed, Section 5.2. Prentice-Hall, Vol. 201, 1995, pp. 90-122.

[17] Taheri-Behrooz, F., Omidi, M., Buckling of Axially Compressed Composite Cylinders with Geometric

Imperfections, Steel and Composite Structures, Vol. 29, No. 4, 2018, pp. 557-67.

[18] Scutaru, M. L., Itu, C., Marin, M., and Grif, H. Ș., Bending Tests Are Used to Determine the Mechanical Properties of The Components of a Composite Sandwich Used in Civil Engineering, Procedia Manufacturing, Vol. 32, 2019, pp. 259-67.

[19] Mohammadi, M., Nazemosadat, S. M. R., and Afsari, A., Modeling and Analysis of a Tractor Diesel Engine Test Stand Structure Using the Finite Element Method, Biomechanism and Bioenergy Research, Vol. 3, No. 2, 2024, pp. 75-87.

[20] Zarei, Y., Afsari, A., Nazemosadat, S. M., and Mohammadi, M., Simulation and Thermo-Mechanical Analysis of AA6063-T5 in FSW by FEM, Journal of Modern Processes in Manufacturing and Production, Vol. 2, 2024, pp. 5.

[21] Mohammadi, M., Nazemosadat, S. M., Fazel, D., and Lari, Y. B., An Integrated Approach for Structural Modeling, Modal Analysis, And Aerodynamic Evaluation of an Electric Vehicle Body Shell Using Finite Element Method and Computational Fluid Dynamics, Materials Today Communications, Vol. 45, 2025, pp. 112331.